64-11

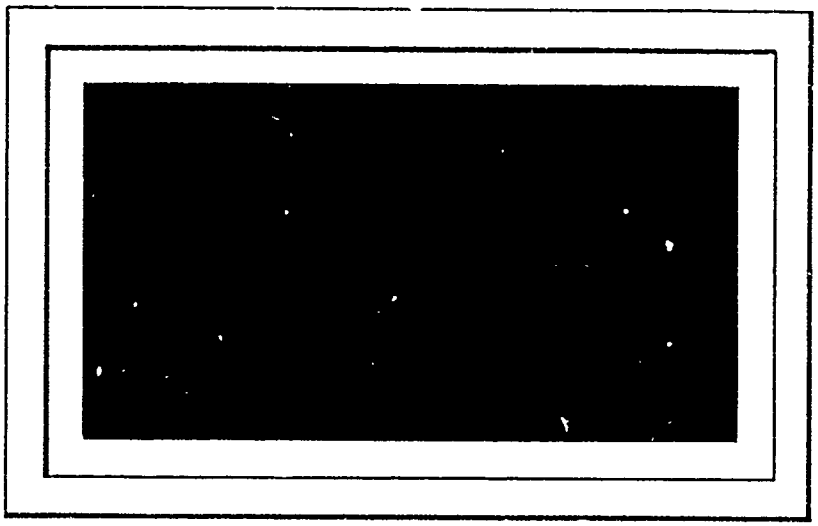

433976

Therm
Advanced
Research, Inc.

100 HUDSON CIRCLE • ITHACA, NEW YORK

THE GENERALIZED ACTUATOR DISK

by

G. R. Hough & D. E. Ordway

TAR-TR 6401 January 1964

This is a paper to be presented at the Second Southeastern Conference on Theoretical and Applied Mechanics to be held in Atlanta, Georgia on March 5-6, 1964. This research was supported by Air Programs, Office of Naval Research, under Contract Nonr-2859(00).

Therm Advanced Research, Inc.
Ithaca, N. Y.

ABSTRACT

Based upon the classical vortex system representation, the induced velocities of a finite-bladed propeller with arbitrary circulation distribution are derived and Fourier analyzed. The zeroth harmonic, or steady component, of the induced velocities is considered in detail and formulas involving only an integration over the blade radius are found. The mathematical equivalence between these results and the conventional actuator disk representation of the propeller is demonstrated. Sample calculations of both the axial and radial velocity components for an arbitrary representative circulation distribution closely approximating the Goldstein optimum are presented. For the special case of a uniformly loaded propeller, expressions for the induced velocity components are given in simple closed form and velocity profiles are compared with the representative results.

INTRODUCTION

The problem of developing suitably simple, yet accurate, expressions for the induced velocity components of a free propeller has long occupied the attention of both the aerodynamicist and the naval architect. Detailed knowledge of the velocity field is extremely important for many applications such as the design of ducted propellers for VTOL aircraft, the evaluation of the interaction between a propeller and a wing immersed in its slipstream, the prediction of the loading on nearby appendages, and the determination of the free-space sound field.

Early approaches to the development of airscrew theory followed two lines: one, the momentum theory of R. E. Froude [1] and W. J. M. Rankine [2] and the related actuator disk concept; and the other, the blade-element theory of W. Froude [3] and S. Drzewiecki [4]. While able to predict propeller performance with some reasonable accuracy, the utility of each theory is limited by basic deficiencies. On the one hand, momentum theory yields neither a relationship between the propeller geometry and the thrust and torque nor any detailed knowledge of the induced velocity field. On the other hand, blade-element theory suffers from the uncertainties involved in assuming the aerodynamic characteristics of the blade sections. It also gives no information regarding the induced

velocity field.

Prediction of the induced velocity field and in particular the local inflow at the propeller plane was finally achieved with the now-classical vortex theory of the propeller. Analyzed in detail by A. Betz and L. Prandtl [5] and S. Goldstein [6] and refined by others [7] & [8], it has enabled, in conjunction with blade-element theory, the accurate determination of propeller performance for the forward flight regime. Still, most calculations of induced velocities using vortex theory are either so complex as to require extensive time on high-speed electronic computers, can not be readily carried out for arbitrary distributions of blade circulation, or are based on the oversimplifying assumption that the number of blades is very large and the flow periodicity may be neglected.

The purpose of this paper is to remove some of the undesirable features of these theories, the results being essentially an extension of part of an earlier analysis for the ducted propeller by D. E. Ordway, M. M. Sluyter and B. U. O. Sonnerup [9]. In outline, we consider a lightly-loaded propeller of arbitrary blade number and circulation distribution operating at zero incidence in a uniform free stream. The propeller is represented by the conventional vortex system and the induced velocities at any field point are determined from the Biot-Savart law. These velocities

are then Fourier analyzed. The zeroth harmonic, or steady component, is considered in detail and identified with the actuator disk, or infinite-blade-number solution. Simplified formulas involving only an integration over the blade radius are derived and sample calculations for an arbitrary representative circulation distribution are carried out. For the special case of uniform propeller loading, the integrations are performed analytically yielding simple closed-form expressions for the velocity field. Several profiles are calculated and compared with those for the representative case.

BASIC FORMULATION

Consider a propeller operating at zero incidence in a uniform, inviscid, incompressible stream of speed U. We assume the propeller to be lightly loaded with N equally spaced blades of radius R which are rotating about their axis at a constant angular velocity Ω. In addition, we assume that both the blade thickness-to-chord and chord-to-radius ratios are negligibly small and, for simplicity, disregard the hub.

A cylindrical propeller-fixed coordinate system (x,r,θ) is chosen such that the propeller disk is normal to the x-axis and is located at $x = 0$, see Fig. 1. In accordance with our assumptions, we can now represent the propeller by

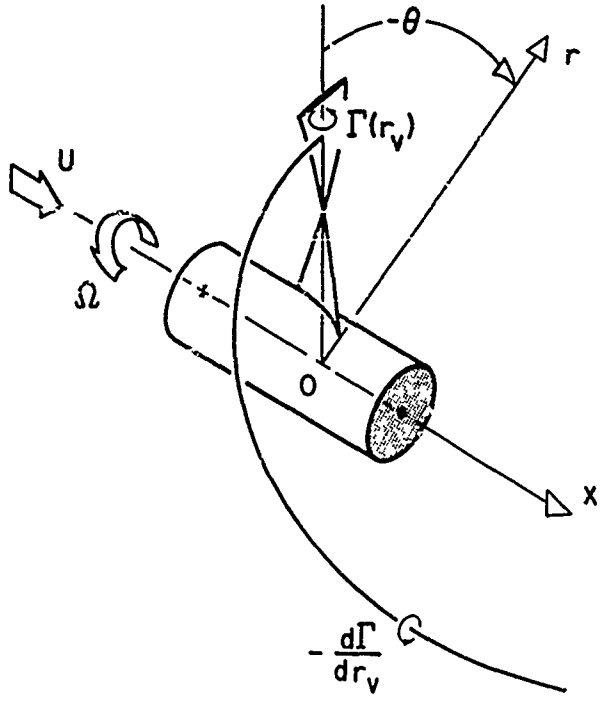

FIGURE 1

COORDINATE SYSTEM AND SCHEMATIC VORTEX REPRESENTATION

the classical model of a bound radial vortex line of strength $\Gamma(r_v)$ for each blade accompanied by a helical sheet of vortices of strength $-d\Gamma/dr_v$ trailing from each line, where r_v is the radial distance to any element of the vortex line. Also consistent with our assumptions, the helical path of the trailing vortex system is determined solely by the incoming free stream with translation U and rotation Ω.

In order to express the induced velocity field it is convenient to introduce three elementary vector velocity fields [9]. These fields or influence functions $\underline{I}_x$, $\underline{I}_r$ and $\underline{I}_\theta$ are due to vortices of unit strength and unit length which lie in the axial, radial and circumferential directions respectively. From the Biot-Savart law we have,

$$\underline{I}_x, \ldots = \underline{i} \times \underline{D} \,/\, 4\pi|\underline{D}|^3 \qquad (1)$$

where $\underline{i}$ is the unit vector in the positive direction of our desired element and $\underline{D}$ is the vector from the element at (x_v, r_v, θ_v) to the field point (x, r, θ). With $\underline{i}_x$, $\underline{i}_r$ and $\underline{i}_\theta$ corresponding to the unit vectors in the x, r and θ directions at the field point, the influence functions reduce to

$$\underline{I}_x = \frac{-r_v \sin(\theta-\theta_v)\underline{i}_r + [r - r_v\cos(\theta-\theta_v)]\underline{i}_\theta}{4\pi D^3}$$

$$\underline{I}_r = \frac{r \sin(\theta-\theta_v)\underline{i}_x - (x-x_v)\sin(\theta-\theta_v)\underline{i}_r - (x-x_v)\cos(\theta-\theta_v)\underline{i}_\theta}{4\pi D^3}$$

$$\underline{I}_\theta = \frac{[r_v - r\cos(\theta-\theta_v)]\underline{i}_x + (x-x_v)\cos(\theta-\theta_v)\underline{i}_r - (x-x_v)\sin(\theta-\theta_v)\underline{i}_\theta}{4\pi D^3}$$

(2)

where

$$D = [(x-x_v)^2 + r^2 + r_v^2 - 2rr_v\cos(\theta-\theta_v)]^{\frac{1}{2}} \tag{3}$$

With these results, the total velocity field for both the bound and trailing vortices may be simply expressed. For q_Γ or the velocity induced by the N bound blade vortex lines, we integrate over each blade and sum the result over all blades, or

$$q_\Gamma = \sum_{\ell=1}^{N} \int_0^R \Gamma(r_v)\, \underline{I}_r(0, r_v, 2\pi\ell/N)\, dr_v \tag{4}$$

Here, the argument of $\underline{I}_r$ is the location of the vortex element, the field point remaining arbitrary for the present, and the index ℓ denotes the ordinal number of the blade.

For $q_{\Gamma'}$ or the velocity induced by the trailing vortices, we first combine an axial and a tangential element appropriately to form an arbitrary helical element lying along the free stream. Then we integrate over the vortex trailing from each radial location. Carrying out a second integration over the radius and

summing over the propeller blades, we arrive at

$$\underline{q}_{\Gamma'} = \sum_{\ell=1}^{N} \int_{0}^{R} -\Gamma'(r_v) \int_{0}^{\infty} (U\,\underline{I}_x + \Omega r_v\,\underline{I}_\theta)\,d\tau\,dr_v \qquad (5)$$

where we have set $\Gamma' \equiv d\Gamma/dr_v$ and the arguments of $\underline{I}_x$ and $\underline{I}_\theta$ are

$$\underline{I}_x = \underline{I}_x(U\tau, r_v, 2\pi\ell/N + \Omega\tau)$$

$$\underline{I}_\theta = \underline{I}_\theta(U\tau, r_v, 2\pi\ell/N + \Omega\tau) \qquad (6)$$

The dummy variable τ represents the time for a trailing element convected by the free stream to travel from the blade to its position downstream and the corresponding integral over τ is equal to the velocity induced by a semi-infinite helical vortex of unit strength, radius r_v and pitch $U/\Omega r_v$.

Superposition of the velocity fields given by Eqs. 4 and 5 determine then, within the limits of our formulation, the total induced velocity at any field point. Within the propeller slipstream these integrals are to be interpreted in the Cauchy Principal Value sense.

FOURIER ANALYSIS OF VELOCITY FIELD

In the coordinate system translating but not rotating with

the propeller, the flow is periodic with time. That is, the velocity at any field point will consist of a steady or time-dependent component plus a superimposed fluctuating component which has a period of $2\pi/N\Omega$. Accordingly, we can express $\underline{q}_r$ and $\underline{q}_{r'}$ in the complex Fourier series

$$\underline{q}_r = U \sum_{m=-\infty}^{\infty} \underline{c}_{r_m}(x,r)\, e^{imN\theta}$$

$$\underline{q}_{r'} = U \sum_{m=-\infty}^{\infty} \underline{c}_{r_m'}(x,r)\, e^{imN\theta} \tag{7}$$

in our propeller-fixed coordinates in which the angular variation is equivalent to the time dependency. The complex Fourier velocity coefficients $\underline{c}_{r_m}$ and $\underline{c}_{r_m'}$ are

$$\underline{c}_{r_m} = \frac{1}{2\pi U} \int_{-\pi}^{\pi} \underline{q}_r\, e^{-imN\theta}\, d\theta$$

$$\underline{c}_{r_m'} = \frac{1}{2\pi U} \int_{-\pi}^{\pi} \underline{q}_{r'}\, e^{-imN\theta}\, d\theta \tag{8}$$

from orthogonality, U being introduced for dimensional purposes.

At this point it is convenient to decompose $\underline{q}_r$, $\underline{q}_{r'}$, $\underline{c}_{r_m}$ and $\underline{c}_{r_m'}$ into their axial, radial and tangential components respectively, or

$$\underline{q}_\Gamma \equiv u_\Gamma \underline{i}_x + v_\Gamma \underline{i}_r + w_\Gamma \underline{i}_\theta$$

$$\underline{q}_{\Gamma'} \equiv u_{\Gamma'} \underline{i}_x + v_{\Gamma'} \underline{i}_r + w_{\Gamma'} \underline{i}_\theta \tag{9}$$

and the components of the complex Fourier velocity coefficients associated with u_Γ ... will be denoted by $c^u_{\Gamma_m}$ ... .

To find, say, the axial component $c^u_{\Gamma_m}$, we replace $\underline{I}_r$ by $\underline{I}_r \cdot \underline{i}_x$ in Eq. 4 using the second of Eqs. 2 . From the first of Eqs. 9 the resulting expression represents u_Γ . If, in turn, we replace $\underline{q}_\Gamma$ by this u_Γ in the first of Eqs. 8 and reverse the order of the r_v and θ integrations, we can carry out the θ integration in terms of Legendre functions [10]. Noting that each blade contributes equally to any harmonic for N identical blades, we obtain

$$c^u_{\Gamma_m} = \frac{-iN}{8\pi^2 U \sqrt{r}} \int_0^R \frac{\Gamma(r_v)}{r_v^{3/2}} \left[Q'_{mN+1/2}(\omega_1) - Q'_{mN-3/2}(\omega_1) \right] dr_v \tag{10}$$

where $Q_{mN+1/2}$ and $Q_{mN-3/2}$ are the Legendre functions of the second kind and half-integer order with argument ω_1 ,

$$\omega_1 \equiv 1 + \frac{x^2 + (r - r_v)^2}{2 r r_v} \tag{11}$$

and the prime ($'$) denotes differentiation with respect to this indicated argument.

The remaining coefficients $c^{v}_{\Gamma_m}$ ... are obtained in similar fashion and are given by

$$c^{v}_{\Gamma_m} = \frac{tNx}{8\pi^2 Ur^{3/2}} \int_0^R \frac{\Gamma(r_v)}{r_v^{3/2}} \left[Q'_{mN+1/2}(\omega_1) - Q'_{mN-3/2}(\omega_1) \right] dr_v$$

$$c^{w}_{\Gamma_m} = \frac{Nx}{8\pi^2 Ur^{3/2}} \int_0^R \frac{\Gamma(r_v)}{r_v^{3/2}} \left[Q'_{mN+1/2}(\omega_1) + Q'_{mN-3/2}(\omega_1) \right] dr_v$$

$$c^{u}_{\Gamma'_m} = \frac{-N\Omega}{8\pi^2 Ur^{3/2}} \int_0^R \frac{\Gamma'(r_v)}{\sqrt{r_v}} \int_0^\infty \left[rQ'_{mN+1/2}(\omega_2) + rQ'_{mN-3/2}(\omega_2) - 2r_v Q'_{mN-1/2}(\omega_2) \right] e^{-tmN\Omega\tau} \, d\tau \, dr_v$$

$$c^{v}_{\Gamma'_m} = \frac{N\Omega}{8\pi^2 Ur^{3/2}} \int_0^R \frac{\Gamma'(r_v)}{\sqrt{r_v}} \int_0^\infty \left[(x - U\tau - \frac{tU}{\Omega}) Q'_{mN+1/2}(\omega_2) + (x - U\tau + \frac{tU}{\Omega}) Q'_{mN-3/2}(\omega_2) \right] e^{-tmN\Omega\tau} \, d\tau \, dr_v$$

$$c^{w}_{\Gamma'_m} = \frac{-N\Omega}{8\pi^2 Ur^{3/2}} \int_0^R \frac{\Gamma'(r_v)}{\sqrt{r_v}} \int_0^\infty \left[(\frac{U}{\Omega} + tx - tU\tau) Q'_{mN+1/2}(\omega_2) + (\frac{U}{\Omega} - tx + tU\tau) Q'_{mN-3/2}(\omega_2) - \frac{2Ur}{\Omega r_v} Q'_{mN-1/2}(\omega_2) \right] e^{-tmN\Omega\tau} \, d\tau \, dr_v$$

(12)

where

$$\omega_2 \equiv 1 + \frac{(x-U\tau)^2+(r-r_v)^2}{2rr_v} \tag{13}$$

For $r > R$, the coefficients for the radial components may be identified with previous results [9].

In general, further analytical simplification of these coefficients to a simple, closed form involving no integrations is not possible. Still they represent an essential simplification. That is, for any harmonic m only $Q'_{mN+1/2}$, $Q'_{mN-1/2}$ and $Q'_{mN-3/2}$ are required, or equivalently $Q_{mN+1/2}$, $Q_{mN-1/2}$, $Q_{mN-3/2}$ and $Q_{mN-5/2}$ from recurrence formulas [10]. This is in contrast to results in terms of elliptic integrals [11] in which the number of necessary functions to be computed rises in geometric progression with m.

The Legendre function of second kind and half order has been examined in detail [10] in connection with recent work on the ducted propeller and extensive tables for orders of $-1/2$ through $21/2$ have been computed [12]. For a fixed value of n, $Q_{n-1/2}(\omega)$ has a simple logarithmic singularity at $\omega = 1$ and decays monotonically to zero as ω increases to infinity. In addition, $Q_{n-1/2}(\omega)$ decays monotonically to zero with increasing n for a given ω.

Altogether, it appears that the Legendre function of second kind and half-integer order is the "natural" function

for the study of the velocity field of a propeller.

STEADY VELOCITY FIELD

If we examine that part of the velocity field corresponding to $m = 0$, considerable simplification in the complex Fourier velocity coefficients is possible. This part corresponds to the steady, or time-independent part of the velocity field. Using $\bar{u}_\Gamma \ldots$ to designate these steady velocity components, we obtain from Eqs. 7, 9, 10 and 12 together with the identity $Q'_{1/2}(\omega) \equiv Q'_{-3/2}(\omega)$, that

$$\bar{u}_\Gamma = 0$$

$$\bar{v}_\Gamma = 0$$

$$\bar{w}_\Gamma = \frac{Nx}{4\pi^2 r^{3/2}} \int_0^R \frac{\Gamma(r_v)}{r_v^{3/2}} Q'_{\frac{1}{2}}(\omega_1)\, dr_v$$

$$\bar{u}_{\Gamma'} = \frac{-N\Omega}{4\pi^2 r^{3/2}} \int_0^R \frac{\Gamma'(r_v)}{\sqrt{r_v}} \int_0^\infty [r Q'_{\frac{1}{2}}(\omega_2) - r_v Q'_{-\frac{1}{2}}(\omega_2)]\, d\tau\, dr_v$$

$$\bar{v}_{\Gamma'} = \frac{N\Omega}{4\pi^2 r^{3/2}} \int_0^R \frac{\Gamma'(r_v)}{\sqrt{r_v}} \int_0^\infty (x - U\tau)\, Q'_{\frac{1}{2}}(\omega_2)\, d\tau\, dr_v$$

$$\bar{w}_{\Gamma'} = \frac{-UN}{4\pi^2 r^{3/2}} \int_0^R \frac{\Gamma'(r_v)}{r_v^{3/2}} \int_0^\infty [r_v Q'_{\frac{1}{2}}(\omega_2) - r Q'_{-\frac{1}{2}}(\omega_2)]\, d\tau\, dr_v \qquad (14)$$

As a result, we find that the bound blade vortices contribute to the tangential velocity only.

The integrations over τ occurring in the expressions for $\bar{u}_{\Gamma'}$, $\bar{v}_{\Gamma'}$ and $\bar{w}_{\Gamma'}$ can be carried out analytically. Since it is the simplest, we first consider $\bar{v}_{\Gamma'}$ and note the relationship

$$(x-U\tau)\, Q'_{\frac{1}{2}}(\omega_2) = -\frac{rr_v}{U}\frac{\partial}{\partial\tau} Q_{\frac{1}{2}}(\omega_2) \tag{15}$$

to obtain

$$\bar{v}_{\Gamma'} = \frac{N\Omega}{4\pi^2 U\sqrt{r}} \int_0^R \Gamma'(r_v)\sqrt{r_v}\, Q_{\frac{1}{2}}(\omega_1)\, dr_v \tag{16}$$

Since x appears only as a squared quantity in the argument ω_1 given by Eq. 11, we see immediately that $\bar{v}_{\Gamma'}$ is symmetric in x. From appropriate expansions of $Q_{\frac{1}{2}}$ for small and large arguments [12], it can be shown that $\bar{v}_{\Gamma'}$ is logarithmically infinite over the propeller disk and vanishes on the propeller axis. Because $\bar{v}_\Gamma = 0$, the same conclusions are true for the total steady induced radial velocity $\bar{v} = (\bar{v}_\Gamma + \bar{v}_{\Gamma'})$.

The $\bar{u}_{\Gamma'}$ and $\bar{w}_{\Gamma'}$ components are reduced by rewriting $Q'_{\frac{1}{2}}(\omega)$ and $Q'_{-\frac{1}{2}}(\omega)$ in their integral form [10], or

$$Q'_{n-\frac{1}{2}}(\omega) = -\int_{-\pi/2}^{\pi/2} \frac{\cos 2n\alpha}{[2(\omega-1)+4\sin^2\alpha]^{3/2}}\, d\alpha \tag{17}$$

The order of the α and τ integrations is then reversed, after which the integrations over τ and then over α may be carried out. The final results are

$$\bar{u}_{\Gamma'} = -\frac{N\Omega}{4\pi^2 U}\int_0^R \Gamma'(r_v)\, K_1(x,r;r_v)\, dr_v$$

$$\bar{w}_{\Gamma'} = -\frac{N}{4\pi^2 r}\int_0^R \Gamma'(r_v)\, K_2(x,r;r_v)\, dr_v \qquad (18)$$

where

$$K_1 = \begin{cases} \pi + \dfrac{x}{2\sqrt{rr_v}}\, Q_{-\frac{1}{2}}(\omega_1) + \dfrac{\pi}{2}\,\Lambda_o(\beta_1,k_1) & \text{IF } r\le r_v,\ x<0 \\ \dfrac{x}{2\sqrt{rr_v}}\, Q_{-\frac{1}{2}}(\omega_1) - \dfrac{\pi}{2}\,\Lambda_o(\beta_1,k_1) & \text{OR } r<r_v,\ x\ge 0 \end{cases}$$

$$\begin{cases} \dfrac{x}{2\sqrt{rr_v}}\, Q_{-\frac{1}{2}}(\omega_1) - \dfrac{\pi}{2}\,\Lambda_o(\beta_1,k_1) & \text{IF } r\ge r_v,\ x<0 \\ \dfrac{x}{2\sqrt{rr_v}}\, Q_{-\frac{1}{2}}(\omega_1) + \dfrac{\pi}{2}\,\Lambda_o(\beta_1,k_1) & \text{OR } r>r_v,\ x\ge 0 \end{cases} \qquad (19)$$

and K_2 is identical to K_1 with the radial inequality signs reversed. $\Lambda_o(\beta_1,k_1)$ is the Heuman Lambda Function [13] with argument β_1 and modulus k_1

$$\beta_1 \equiv \sin^{-1}\frac{x}{\sqrt{x^2+(r-r_v)^2}}\ , \quad k_1 \equiv \sqrt{\frac{4rr_v}{x^2+(r+r_v)^2}} \qquad (20)$$

Eqs. 18 can be still further simplified if we integrate by parts with $\Gamma' dr_v$ as the differential and use the relationship which we have found,

$$\frac{\partial \Lambda_o}{\partial r_v} = \pm \frac{1}{\pi} \frac{x}{(xr_v)^{3/2}} [r_v Q'_{-\frac{1}{2}}(\omega_1) + x Q_{-\frac{1}{2}}(\omega_1)] \; ; \begin{cases} + & \text{IF} \quad r<r_v \\ - & \text{IF} \quad r>r_v \end{cases} \tag{21}$$

Since the circulation must vanish at the tip, we find for $\bar{u}_{\Gamma'}$

$$\frac{N\times\Omega}{4\pi^2 U r^{3/2}} \int_0^R \frac{\Gamma(r_v)}{\sqrt{r_v}} Q'_{-\frac{1}{2}}(\omega_1)\, dr_v \; ; \begin{cases} \text{IF} \quad r>R \; , & -\infty \leq x \leq \infty \\ \text{OR} \quad r \leq R \; , & x<0 \end{cases}$$

$$\bar{u}_{\Gamma'} = \frac{N\Omega\Gamma(r)}{2\pi U} + \frac{N\times\Omega}{4\pi^2 U r^{3/2}} \int_0^R \frac{\Gamma(r_v)}{\sqrt{r_v}} Q'_{-\frac{1}{2}}(\omega_1)\, dr_v \; ; \quad \text{IF} \quad r \leq R \; , \; x>0$$

$$\frac{N\Omega\Gamma(r)}{4\pi U} \; ; \quad \text{IF} \quad r \leq R \; , \; x=0 \tag{22}$$

From the first of Eqs. 14 and Eqs. 22, we see the following. At radial stations greater than the propeller radius, the total steady axial induced velocity $\bar{u} = (\bar{u}_\Gamma + \bar{u}_{\Gamma'})$ is antisymmetric with respect to x. At the propeller plane it vanishes off the propeller disk and has the same shape as the blade circulation distribution over the propeller disk, cf. Refs. [14] and [15]. Far down in the slipstream, $\bar{u}$ is twice that at the propeller plane, the same as in momentum theory.

For $\bar{w}_{\Gamma'}$ we get

$$\frac{-Nx}{4\pi^2 r^{3/2}} \int_0^R \frac{\Gamma(r_v)}{r_v^{3/2}} Q'_{\frac{1}{2}}(\omega_1)\, dr_v \quad ; \begin{cases} \text{IF} & r>R\ ,\ -\infty \leq x \leq \infty \\ \text{OR} & r \leq R\ ,\ x<0 \end{cases}$$

$$\bar{w}_{\Gamma'} = \frac{N\Gamma(r)}{2\pi r} - \frac{Nx}{4\pi^2 r^{3/2}} \int_0^R \frac{\Gamma(r_v)}{r_v^{3/2}} Q'_{\frac{1}{2}}(\omega_1)\, dr_v \quad ; \quad \text{IF} \quad r \leq R\ ,\ x>0$$

$$\frac{N\Gamma(r)}{4\pi r} \quad ; \quad \text{IF} \quad r \leq R\ ,\ x=0 \qquad (23)$$

The total steady induced tangential velocity $\bar{w} = (\bar{w}_{\Gamma}+\bar{w}_{\Gamma'})$ from the third of Eqs. 14 and Eqs. 23 is, then,

$$0 \quad ; \begin{cases} \text{IF} & r>R\ ,\ -\infty \leq x \leq \infty \\ \text{OR} & r \leq R\ ,\ x<0 \end{cases}$$

$$\bar{w} = \frac{N\Gamma(r)}{2\pi r} \quad ; \quad \text{IF} \quad r \leq R\ ,\ x>0$$

$$\frac{N\Gamma(r)}{4\pi r} \quad ; \quad \text{IF} \quad r \leq R\ ,\ x=0 \qquad (24)$$

That is, the tangential velocity vanishes everywhere outside the propeller slipstream and is proportional to $\Gamma(r)/r$ inside the slipstream. This is the same result as we can derive directly by application of Kelvin's Theorem using a circular path about the x-axis.

The results of Eqs. 22 and 24 as regards to the inflow at the propeller plane are especially noteworthy. In particular, $\bar{u}/\bar{w} = \Omega r/U$ and so from the velocity diagram at a blade section, the resultant induced velocity vector is perpendicular to the resultant free stream vector $(U\underline{i}_x - \Omega r \underline{i}_\theta)$. This is the same as Moriya [7] found for the total inflow, or steady plus higher harmonics. Therefore, we conclude it must be true for these harmonics as well.

In summary, the total axial component of the steady induced velocity field is determined by Eqs. 22 and $\bar{u}_\Gamma = 0$, the radial component by Eq. 16 and $\bar{v}_\Gamma = 0$, and the tangential component by Eqs. 24. We see that these relations if expressed in non-dimensional form would be <u>independent of the blade number</u> for a fixed advance ratio $J \equiv U/\Omega R$ and disk loading

$$\frac{dC_T}{d(r/R)} = \frac{2N}{\pi J} \frac{r}{R} \frac{\Gamma}{UR} \tag{25}$$

where C_T is the propeller thrust coefficient. Consequently, on a physical basis they must be equal to the respective components of the $\lim_{N\to\infty} (\underline{q}_\Gamma + \underline{q}_{\Gamma'})$ of Eqs. 7 subject to the same conditions. This limit corresponds to the velocity field associated with what we now define as the GENERALIZED ACTUATOR DISK, i. e., the precise mathematical definition of the actuator disk as opposed to a model with certain characteristics assumed a priori.

REPRESENTATIVE BLADE CIRCULATION DISTRIBUTION VELOCITY PROFILES

To illustrate the theory, we have calculated several $\bar{u}$ and $\bar{v}$ profiles for the representative blade circulation distribution given by

$$\frac{\Gamma}{UR} = A \frac{r}{R} \sqrt{1 - \frac{r}{R}} \tag{26}$$

This particular Γ was contrived because it simplifies the calculations and approximates the familiar Goldstein optimum distribution [6] quite well, particularly the proper square root behavior at the tip, see Fig. 2. The constant A is proportional to the propeller thrust coefficient C_T. By substituting Eq. 26 into Eq. 25 and integrating, we have

$$A = \frac{105}{32} \frac{\pi J}{N} C_T \tag{27}$$

where $C_T \equiv T/\pi R^2 \, \frac{1}{2}\rho U^2$. T is the propeller thrust and ρ is the fluid density.

The axial and radial velocities were calculated on a CDC 1604 digital computer from Eqs. 22 and Eq. 16. The results in terms of C_T from Eq. 27 are tabulated in Tables 1 and 2 and sketched in Figs. 3 and 4 respectively. Several features are prominent in addition to those observed previously. From Fig. 3 the steady induced axial velocity off the propeller disk

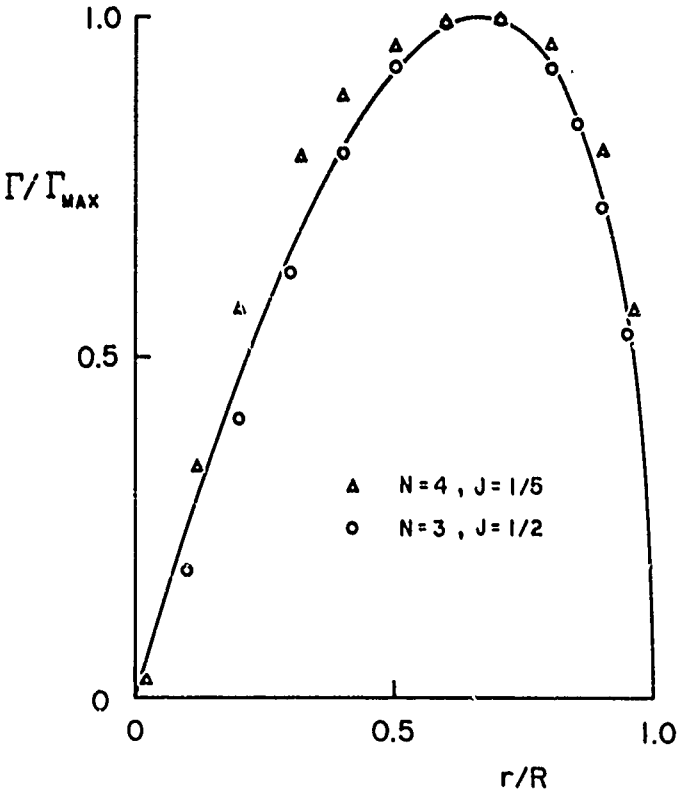

FIGURE 2

COMPARISON OF REPRESENTATIVE CIRCULATION DISTRIBUTION WITH GOLDSTEIN OPTIMUM

	$(\bar{u}/U)/C_T$								
$\frac{r}{R}$ \ $\frac{x}{R}$	-2.0	-1.0	-0.5	-0.1	0	0.1	0.5	1.0	2.0
0	0.026	0.072	0.130	0.122	0	-0.122	-0.130	-0.072	-0.026
0.1	0.026	0.072	0.130	0.136	0.078	0.020	0.026	0.084	0.130
0.2	0.026	0.072	0.131	0.165	0.147	0.128	0.163	0.222	0.268
0.3	0.026	0.070	0.131	0.197	0.206	0.215	0.281	0.342	0.386
0.4	0.025	0.068	0.129	0.224	0.254	0.285	0.379	0.440	0.483
0.5	0.025	0.066	0.126	0.242	0.290	0.338	0.454	0.515	0.555
0.6	0.024	0.062	0.119	0.250	0.311	0.373	0.503	0.561	0.598
0.7	0.023	0.058	0.110	0.242	0.315	0.387	0.519	0.571	0.606
0.8	0.022	0.054	0.098	0.215	0.293	0.372	0.489	0.533	0.564
0.9	0.022	0.050	0.085	0.162	0.233	0.305	0.382	0.417	0.445
1.0	0.021	0.045	0.070	0.088	0	-0.088	-0.070	-0.045	-0.021
1.1	0.020	0.040	0.057	0.040	0	-0.040	-0.057	-0.040	-0.020
1.2	0.019	0.036	0.046	0.022	0	-0.022	-0.046	-0.036	-0.019
1.5	0.016	0.025	0.023	0.007	0	-0.007	-0.023	-0.025	-0.016
2.0	0.011	0.013	0.009	0.002	0	-0.002	-0.009	-0.013	-0.011
3.0	0.005	0.004	0.003	0.001	0	-0.001	-0.003	-0.004	-0.005
5.0	0.002	0.001	0.001	0.000	0	-0.000	-0.001	-0.001	-0.002

TABLE 1

STEADY INDUCED AXIAL VELOCITY FOR
$\Gamma/RU = A(r/R)\sqrt{1-(r/R)}$

	$(\bar{v}/U)/c_T$								
$\frac{r}{R}$ \ $\frac{x}{R}$	±0.05	±0.1	±0.2	±0.4	±0.6	±0.8	±1.0	±1.5	±2.0
0	0	0	0	0	0	0	0	0	0
0.1	0.036	0.020	0.004	-0.006	-0.007	-0.005	-0.004	-0.002	-0.001
0.2	0.044	0.025	0.002	-0.013	-0.014	-0.011	-0.009	-0.004	-0.002
0.3	0.032	0.014	-0.008	-0.022	-0.021	-0.017	-0.013	-0.006	-0.003
0.4	0.006	-0.008	-0.025	-0.033	-0.029	-0.022	-0.017	-0.008	-0.004
0.5	-0.031	-0.040	-0.048	-0.046	-0.037	-0.027	-0.020	-0.010	-0.005
0.6	-0.077	-0.078	-0.075	-0.060	-0.044	-0.032	-0.024	-0.011	-0.006
0.7	-0.128	-0.121	-0.103	-0.072	-0.051	-0.037	-0.027	-0.013	-0.007
0.8	-0.183	-0.163	-0.128	-0.083	-0.056	-0.040	-0.029	-0.014	-0.008
0.9	-0.234	-0.196	-0.144	-0.088	-0.059	-0.042	-0.031	-0.015	-0.008
1.0	-0.238	-0.194	-0.142	-0.089	-0.060	-0.043	-0.032	-0.016	-0.009
1.1	-0.167	-0.155	-0.126	-0.084	-0.059	-0.043	-0.032	-0.017	-0.009
1.2	-0.125	-0.120	-0.106	-0.078	-0.057	-0.042	-0.032	-0.017	-0.010
1.5	-0.068	-0.067	-0.064	-0.055	-0.045	-0.036	-0.029	-0.017	-0.010
2.0	-0.035	-0.034	-0.034	-0.032	-0.029	-0.025	-0.022	-0.015	-0.010
3.0	-0.014	-0.014	-0.014	-0.014	-0.014	-0.013	-0.012	-0.010	-0.008
5.0	-0.005	-0.005	-0.005	-0.005	-0.005	-0.005	-0.005	-0.004	-0.004

TABLE 2

STEADY INDUCED RADIAL VELOCITY FOR

$\Gamma/RU = A(r/R)\sqrt{1-(r/R)}$

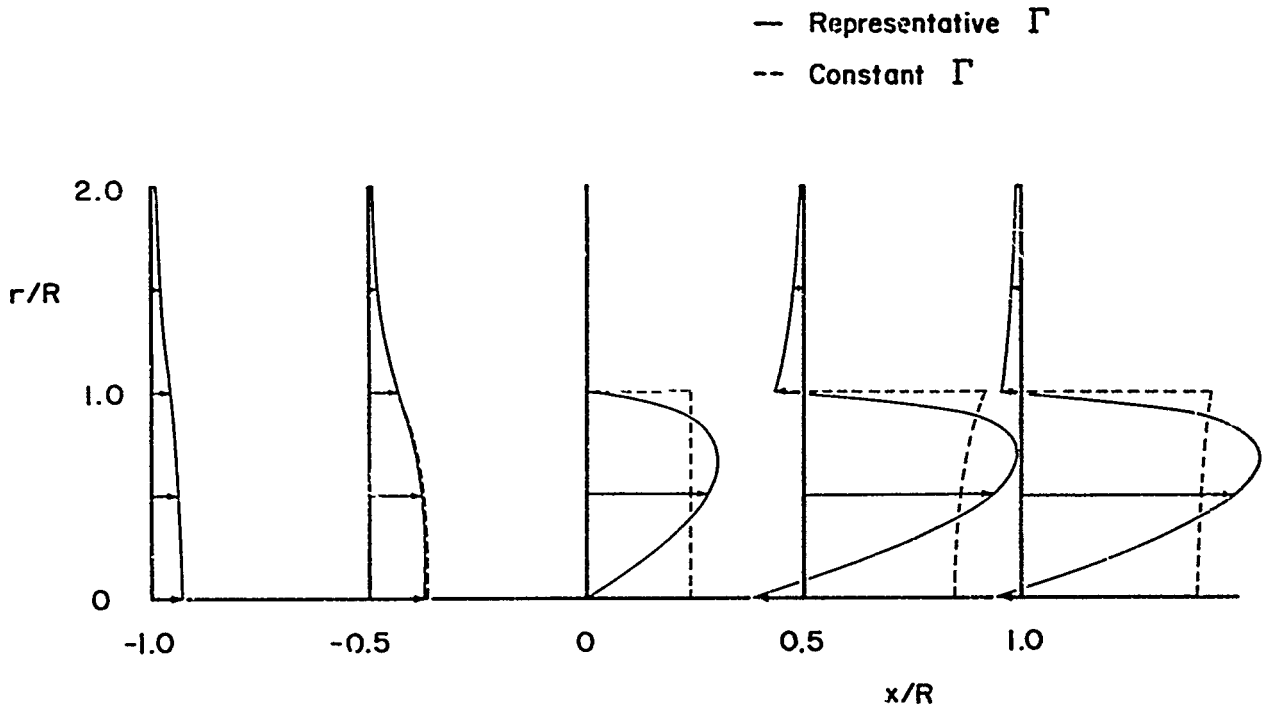

FIGURE 3

COMPARISON OF STEADY AXIAL VELOCITY PROFILES

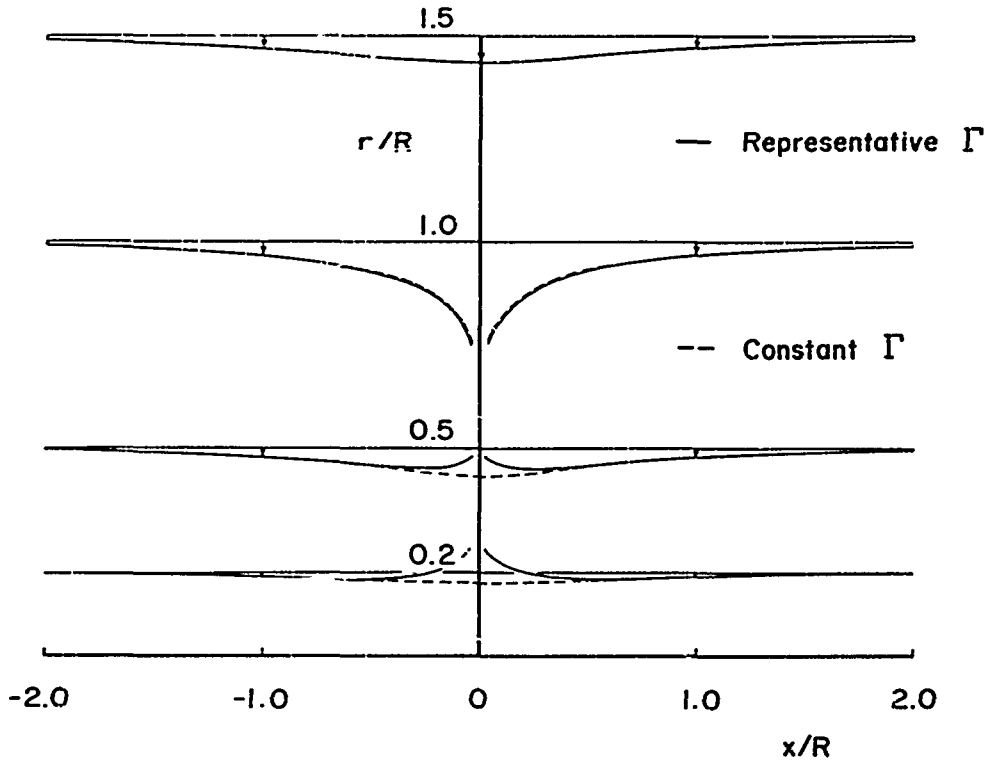

FIGURE 4

COMPARISON OF STEADY RADIAL VELOCITY PROFILES

vanishes in the propeller plane, leaving the free stream unperturbed except for the radial velocity. Inside the slipstream $\bar{u}$ quickly approaches within a blade radius twice its value at the propeller plane and decays just as fast upstream. From Fig. 4 we see a rapid change in the radial velocity in the immediate vicinity of the propeller plane and a smoother variation farther away. Within a certain radius from the propeller axis and near the propeller plane, $\bar{v}$ reverses and the radial flow is outward. This reversal is due to the influence of the trailing vortices inboard of the maximum value of Γ which are of opposite sign to those outboard. At axial stations near the propeller plane the velocity is still appreciable for large radial distances, whereas the profile quickly decays with large axial distance away from the propeller in the vicinity of the propeller axis.

CONSTANT BLADE CIRCULATION DISTRIBUTION VELOCITY PROFILES

For the special case in which the circulation distribution over the propeller blade is constant, the results for the steady induced velocities can be put in simple, closed form because fundamentally they are the "building blocks" for the case of arbitrary circulation.

With $\Gamma(r) = \Gamma_c$, it is easiest to reduce $\bar{u}$ by returning to the intermediate form of $\bar{u}_\Gamma$, or the first of Eqs. 18.

This yields only a contribution from the tip which, together with $\bar{u}_\Gamma = 0$, gives

$$\frac{N\Gamma_c\Omega}{4\pi^2 U}\left[\pi + \frac{x}{2\sqrt{rR}}\, Q_{-\frac{1}{2}}(\omega_3) + \frac{\pi}{2}\,\Lambda_o(\beta_2,k_2)\right] \; ; \begin{cases} \text{IF} & r\leq R \;,\; x<0 \\ \text{OR} & r<R \;,\; x\geq 0 \end{cases}$$

$$\bar{u} =$$

$$\frac{N\Gamma_c\Omega}{4\pi^2 U}\left[\frac{x}{2\sqrt{rR}}\, Q_{-\frac{1}{2}}(\omega_3) - \frac{\pi}{2}\,\Lambda_o(\beta_2,k_2)\right] \; ; \begin{cases} \text{IF} & r\geq R \;,\; x<0 \\ \text{OR} & r>R \;,\; x\geq 0 \end{cases} \tag{28}$$

where

$$\omega_3 \equiv 1 + \frac{x^2+(r-R)^2}{2rR}$$

$$\beta_2 \equiv \sin^{-1}\frac{x}{\sqrt{x^2+(r-R)^2}} \quad , \quad k_2 \equiv \sqrt{\frac{4rR}{x^2+(r+R)^2}} \tag{29}$$

Across the cylinder $(r=R \;,\; x\geq 0)$, there is a constant jump in velocity of $N\Gamma_c\Omega/2\pi U$ which can be identified as the average vorticity per unit length in the axial direction resulting from the trailing tip vortices or $(N\Gamma_c/2\pi R)/J$. Over the propeller disk $\bar{u}$ becomes $N\Gamma_c\Omega/4\pi U$, or one-half of its value far downstream, the same as in momentum theory.

The radial component follows from Eq. 16 and $\bar{v}_\Gamma = 0$ in similar fashion, or

$$\bar{v} = -\frac{N\Gamma_c\Omega}{4\pi^2 U}\sqrt{\frac{R}{r}}\; Q_{\frac{1}{2}}(\omega_3) \tag{30}$$

As opposed to the representative case, $\bar{v}$ now is finite over the propeller disk except at the tip. Furthermore, it does not reverse sign as the only trailing vortices of opposite sign to the tip vortices lie along the propeller axis and do not induce any radial flow.

These velocities have been calculated and are tabulated in Tables 3 and 4. They are compared back with the results for the representative circulation distribution in Figs. 3 and 4. From the figures we see that for radial stations less than the propeller radius the results are not in close agreement, the disparity being most pronounced within the propeller slipstream. However, there is no significant difference between the two results for $r/R > 1.5$.

While the condition of constant circulation along the entire blade is physically impossible [14], we can conclude that the determination of the propeller induced velocities outside the slipstream may be satisfactorily approximated by assuming such a circulation distribution. On the other hand, prediction of the flow field within the slipstream as well as in the immediate vicinity ahead of the propeller plane will be in serious error if a constant blade circulation is assumed.

IDENTIFICATION WITH ACTUATOR DISK SOLUTION

As we said earlier, the assumption is often made simply a priori that the blade number N is infinite and so, the

	$(\bar{u}/U)/c_T$								
$\frac{r}{R}$ \ $\frac{x}{R}$	-2.0	-1.0	-0.5	-0.1	0	0.1	0.5	1.0	2.0
0	0.026	0.073	0.138	0.225	0.250	0.275	0.362	0.427	0.474
0.1	0.026	0.073	0.138	0.225	0.250	0.275	0.362	0.427	0.474
0.2	0.026	0.072	0.136	0.224	0.250	0.276	0.364	0.428	0.474
0.3	0.026	0.070	0.133	0.223	0.250	0.277	0.367	0.430	0.474
0.4	0.025	0.068	0.129	0.222	0.250	0.278	0.371	0.432	0.475
0.5	0.025	0.065	0.124	0.219	0.250	0.281	0.377	0.435	0.475
0.6	0.024	0.062	0.116	0.215	0.250	0.285	0.384	0.438	0.476
0.7	0.023	0.058	0.107	0.209	0.250	0.291	0.393	0.442	0.477
0.8	0.022	0.054	0.096	0.197	0.250	0.303	0.404	0.446	0.478
0.9	0.022	0.049	0.084	0.170	0.250	0.330	0.416	0.451	0.478
1.0	0.021	0.045	0.070	0.108	0.125	0.142	0.180	0.205	0.229
1.1	0.020	0.040	0.058	0.047	0	-0.047	-0.058	-0.040	-0.020
1.2	0.019	0.036	0.046	0.024	0	-0.024	-0.046	-0.036	-0.019
1.5	0.016	0.025	0.024	0.007	0	-0.007	-0.024	-0.025	-0.016
2.0	0.011	0.013	0.009	0.002	0	-0.002	-0.009	-0.013	-0.011
3.0	0.005	0.004	0.003	0.001	0	-0.001	-0.003	-0.004	-0.005
5.0	0.002	0.001	0.001	0.000	0	-0.000	-0.001	-0.001	-0.002

TABLE 3

STEADY INDUCED AXIAL VELOCITY FOR

Γ/RU = CONSTANT

$(\bar{v}/U)/c_T$

$\frac{r}{R}$ \ $\frac{x}{R}$	± 0.05	± 0.1	± 0.2	± 0.4	± 0.6	± 0.8	± 1.0	± 1.5	± 2.0
0	0	0	0	0	0	0	0	0	0
0.1	-0.013	-0.012	-0.012	-0.010	-0.008	-0.006	-0.004	-0.002	-0.001
0.2	-0.025	-0.025	-0.024	-0.020	-0.016	-0.012	-0.009	-0.004	-0.002
0.3	-0.039	-0.038	-0.036	-0.030	-0.023	-0.017	-0.013	-0.006	-0.003
0.4	-0.053	-0.052	-0.049	-0.040	-0.031	-0.023	-0.017	-0.008	-0.004
0.5	-0.069	-0.068	-0.064	-0.051	-0.038	-0.028	-0.020	-0.010	-0.005
0.6	-0.088	-0.086	-0.079	-0.061	-0.045	-0.032	-0.024	-0.011	-0.006
0.7	-0.110	-0.107	-0.096	-0.071	-0.050	-0.036	-0.026	-0.013	-0.007
0.8	-0.140	-0.134	-0.114	-0.079	-0.055	-0.039	-0.029	-0.014	-0.008
0.9	-0.187	-0.168	-0.131	-0.084	-0.058	-0.041	-0.030	-0.015	-0.008
1.0	-0.245	-0.190	-0.136	-0.086	-0.059	-0.042	-0.031	-0.016	-0.009
1.1	-0.177	-0.159	-0.125	-0.083	-0.058	-0.042	-0.032	-0.017	-0.009
1.2	-0.129	-0.123	-0.107	-0.077	-0.056	-0.042	-0.032	-0.017	-0.010
1.5	-0.068	-0.068	-0.064	-0.055	-0.045	-0.036	-0.029	-0.017	-0.010
2.0	-0.035	-0.034	-0.034	-0.032	-0.029	-0.025	-0.022	-0.015	-0.010
3.0	-0.015	-0.014	-0.014	-0.014	-0.014	-0.013	-0.012	-0.010	-0.008
5.0	-0.005	-0.005	-0.005	-0.005	-0.005	-0.005	-0.005	-0.004	-0.003

TABLE 4

STEADY INDUCED RADIAL VELOCITY FOR
Γ/RU = CONSTANT

propeller is replaced by an "imaginary" disk across which the axial velocity is continuous while the fluid pressure is suddenly increased in passing from one side to the other. In the absence of swirl this permits the use of appropriate distributions of ring vortices or sources to represent the flow [16]. These representations can be related to our solution for the steady induced flow field of the finite-bladed propeller.

First consider the ring vortex representation for the axial component of the induced velocity. The stream function Ψ for a ring vortex of unit strength is

$$\Psi = \frac{1}{2\pi} \sqrt{r r_v}\, Q_{\frac{1}{2}}(\omega_4)$$

$$\omega_4 = 1 + \frac{(x-x_v)^2+(r-r_v)^2}{2rr_v} \tag{31}$$

where x_v is the axial location of the ring and r_v is the ring radius. The corresponding induced axial velocity becomes after simplification,

$$\frac{1}{r}\frac{\partial \Psi}{\partial r} = \frac{1}{2\pi r^{3/2}\sqrt{r_v}} \left[r Q'_{\frac{1}{2}}(\omega_4) - r_v Q'_{-\frac{1}{2}}(\omega_4) \right] \tag{32}$$

With τ replaced by x_v/U, we see that $\bar{u}$ from Eqs. 14 is equal to the slipstream integration of Eq. 32 weighted by the

vortex strength $-N\Omega d\Gamma(r_v)dx_v/2\pi U$. But this agrees exactly with the usual expression for the induced axial velocity associated with the actuator disk in terms of ring vortices: Take for simplicity the case of uniform loading which requires only a single semi-infinite solenoid of such vortices of radius R . From momentum theory, the ratio of the total velocity in the ultimate slipstream to U is $\sqrt{1+C_T}$, or linearized for light loading $(1+\frac{1}{2}C_T)$; cf. Table 3, $\bar{u}/UC_T = 0.25$ at $x=0$, $r/R<1$ and $\bar{u}/UC_T \to 0.5$ as $x\to\infty$, $r/R<1$. Consequently, $\frac{1}{2}UC_T dx_v$ is the proper vortex strength. On the other hand, $d\Gamma(r_v) = -\Gamma_c$ at R and the vortex strength from the expression above is then simply $N\Omega\Gamma_c dx_v/2\pi U$ which properly corresponds to the velocity jump noted for Eqs. 28 times dx_v . Substituting $C_T = (N/\pi J)(\Gamma_c/UR) = N\Omega\Gamma_c/\pi U^2$ from integration of Eq. 25, we arrive at $\frac{1}{2}UC_T dx_v$ again. The case of arbitrary loading follows from the superposition of such solenoids of radius r_v .

If we examine in turn the radial velocity of a vortex ring or $\partial\Psi/r\partial x$ from Eq. 31 and compare it similarly with $\bar{v}$ from Eqs. 14, we obtain the identical result. With regard to $\bar{w}$, the swirl is generally omitted from the actuator disk concept. But if we incorporate a distribution of concentric cylinders of semi-infinite straight vortices parallel to the x-axis, we can establish the equivalence as for $\bar{u}$ and $\bar{v}$.

For the representation of the actuator disk by the distribution of ring sources on the propeller disk, we can proceed formally to prove the equivalence as for the vortex rings. Inasmuch as the equivalence between the ring sources and vortex rings has already been established [16] & [17], this is not necessary. If desired, though, Eqs. 22 are best for the axial velocity. For the radial velocity, integrate Eq. 16 by parts. The respective velocities for a ring source follow from the potential Φ per unit source strength,

$$\Phi = -\frac{1}{4\pi^2}\frac{1}{\sqrt{rr_v}}Q_{-\frac{1}{2}}(\omega_1) \tag{33}$$

where $x = 0$ is the axial location of the ring and r_v, the radius. We find that outside the propeller slipstream the velocities are equal and the required strength of the ring source is $-N\Omega r_v\Gamma(r_v)dr_v/U$, i. e., a ring sink. Inside the slipstream the radial velocities are the same but the axial velocities differ by the constant $N\Omega\Gamma(r)/2\pi U$, cf. Eq. 22, since $\bar{u}$ for the ring source is antisymmetric in x everywhere.

CONCLUSIONS

From our study of the induced velocity field of a finite-bladed propeller with arbitrary circulation distribution, we have concluded the following:

Relatively simple forms for the Fourier coefficients of the axial, radial and tangential velocities can be obtained involving only Legendre functions of the second kind and half integer order. These appear to be the "natural" functions for use in propeller theory.

A comparison of the steady velocity profiles for both a representative and a constant circulation distribution reveals that the two results in general agree closely outside the propeller slipstream. However, calculation of the field immediately ahead of the propeller as well as inside the slipstream under the assumption of uniform loading may lead to serious errors.

For the special case of constant circulation, the steady induced velocity components can be expressed in closed form involving no integration.

The axial and radial induced velocities for the conventional actuator disk are established as exactly equal to their steady counterparts for a finite-bladed propeller, provided the advance ratio and the disk loading are the same.

REFERENCES

1. R. E. Froude, "On the Part Played in Propulsion by Differences of Fluid Pressure", Trans. Inst. Nav. Arch., Vol. 30, 1889, p. 390.

2. W. J. M. Rankine, "On the Mechanical Principles of the Action of Propellers", Trans. Inst. Nav. Arch., Vol. 6, 1865, p. 13.

3. W. Froude, "On the Elementary Relation between Pitch Slip, and Propulsive Efficiency", Trans. Inst. Nav. Arch., Vol. 19, 1878, p. 47.

4. S. Drzewiecki, "Théorie Générale de l'Hélice", Paris, 1920.

5. A. Betz, "Schraubenpropeller mit geringstem Energieverlust", Appendix by L. Prandtl, Göttinger Nachr., 1919, p. 193.

6. S. Goldstein, "On the Vortex Theory of Screw Propellers", Proceedings of the Royal Society of London, A, Vol. 123, 1929, p. 440.

7. T. Moriya, "Selected Scientific and Technical Papers", Moriya Memorial Committee, University of Tokyo, Tokyo, August 1959.

8. M. Iwasaki, "Diagrams for Use in Calculation of Induced Velocity by Propeller", Reports of Research Institute for Applied Mechanics, Kyushu University, Fukuoka City, Vol. VI, No. 23, 1958.

9. D. E. Ordway, M. M. Sluyter and B. U. O. Sonnerup, "Three-Dimensional Theory of Ducted Propellers", THERM, Incorporated, TAR-TR 602, August 1960.

10. B. U. O. Sonnerup, "Expression as a Legendre Function of an Elliptic Integral Occurring in Wing Theory", THERM, Incorporated, TAR-TN 59-1, November 1960.

11. J. P. Breslin and S. Tsakonas, "Marine Propeller Pressure Field Including Effects of Loading and Thickness", SNAME Transactions, Vol. 67, 1959, p. 386.

12. M. M. Sluyter, "A Computational Program and Extended Tabulation of Legendre Functions of Second Kind and Half Order", THERM, Incorporated, TAR-TR 601, October 1960.

13. P. F. Byrd and M. D. Friedman, "Handbook of Elliptic Integrals for Engineers and Physicists", Springer-Verlag, Berlin, 1954.

14. H. Glauert, "Airplane Propellers", Division L of "Aerodynamic Theory", Edited by W. F. Durand, Dover Publications, New York, 1963.

15. R. H. Miller, "Rotor Blade Harmonic Air Loading", IAS Paper No. 62-82, January 1962.

16. L. Meyerhoff and A. B. Finkelstein, "On Theories of the Duct Shape for a Ducted Propeller", Polytechnic Institute of Brooklyn, PIBAL Report No. 484, August 1958.

17. D. Küchemann and J. Weber, "Aerodynamics of Propulsion", McGraw-Hill, New York, 1953.

PRINCIPAL NOMENCLATURE

C_T	propeller thrust coefficient, $T/\pi R^2 \frac{1}{2}\rho U^2$
$\underline{C}_{\Gamma_m}$, $\underline{C}_{\Gamma_m}'$	complex Fourier velocity coefficients for $\underline{q}_\Gamma$ and $\underline{q}_{\Gamma'}$
J	propeller advance ratio, $U/\Omega R$
m	harmonic number
N	number of propeller blades
$\bar{Q}_{n-\frac{1}{2}}(\omega)$	Legendre function of second kind and half-integer order of argument ω
$\underline{q}_\Gamma$	vector velocity induced by bound blade vortices
$\underline{q}_{\Gamma'}$	vector velocity induced by blade trailing vortices
R	propeller radius
U	forward flight velocity
u,v,w	axial, radial and tangential components respectively of induced velocity
x,r,θ	cylindrical propeller-fixed coordinate system
$\Gamma(r)$	propeller blade circulation
$\Lambda_o(\beta,k)$	Heuman's Lambda function of argument β and modulus k

Ω	propeller angular velocity
$(\,)'$	differentiation of a function with respect to its indicated argument
$(\bar{\ })$	zeroth harmonic or steady part of induced velocity

Approved Distribution List for Unclassified
Technical Reports Issued Under Contract Nonr-4357(00)

Chief, Bureau of Naval Weapons
(RAAD-3)
Department of the Navy
Washington, D. C. 20360

Chief, Bureau of Naval Weapons
(RAAD-22)
Department of the Navy
Washington, D. C. 20360

Chief, Bureau of Naval Weapons
(RAAD-32)
Department of the Navy
Washington, D. C. 20360

Chief, Bureau of Naval Weapons
(RAAD-33)
Department of the Navy
Washington, D. C. 20360

Chief, Bureau of Naval Weapons
(RAAD-34)
Department of the Navy
Washington, D. C. 20360

Chief, Bureau of Naval Weapons
(RA-4)
Department of the Navy
Washington, D. C. 20360

Chief, Bureau of Naval Weapons
(R-55)
Department of the Navy
Washington, D. C. 20360

Chief, Bureau of Naval Weapons
(RRRE-4)
Department of the Navy
Washington, D. C. 20360

Commanding Officer
U. S. Army Transportation Research
Command
Fort Eustis, Virginia
ATTN: SMOFE-TD (1 copy)
Research Reference Center (1 copy)

Chief of Naval Research (Code 461)
Department of the Navy
Washington, D. C. 20360 (6 copies)

Chief of Naval Research (Code 438)
Department of the Navy
Washington, D. C. 20360

Commanding Officer
Office of Naval Research Branch
Office
Navy #100, Box 39, F.P.O.
New York, New York (2 copies)

Commanding Officer
Office of Naval Research Branch
Office
346 Broadway
New York 13, New York

Director
Naval Research Laboratory
Technical Information Office
Washington, D. C. 20390 (6 copies)

Commander
Army Material Command
ATTN: AMCRD-RS-PE-A
Department of the Army
Washington, D. C. 20315

Commanding Officer and Director
David Taylor Model Basin
Aerodynamics Laboratory Library
Washington, D. C. 20007

Army Research Office
Physical Sciences Division
ATTN: Mr. R. Ballard
3045 Columbia Pike
Arlington, Virginia 20310

U. S. Air Force (SRGL)
Office of Scientific Research
Washington 25, D. C.

Research and Technology Division
ATTN: SESSC (Mr. Lindenbaum)
Wright-Patterson AFB, Ohio 45433

Defense Documentation Center
Hq., Cameron Station
Building #5
Alexandria, Virginia 22314
(20 copies)

National Aeronautics and Space
Administration
600 Independence Avenue, S.W.
ATTN: Code RA, Code RAD
Washington, D. C. 20546 (2 copies)

Library
American Institute of Aeronautics
and Astronautics
Two East 64 Street
New York 21, New York (2 copies)

Research and Technology Division
ATTN: FDM (Mr. Antonatos)
Wright-Patterson AFB, Ohio 45433

Cornell Aeronautical Lab., Inc.
4455 Genesee Street
Buffalo 21, New York
ATTN: Technical Director
Mr. H. A. Cheilek

Collins Radio Company
Cedar Rapids, Iowa
ATTN: Dr. A. Lippisch

Mr. A. M. O. Smith, Supervisor
Aerodynamics Research Group
Aircraft Division
Douglas Aircraft Co., Inc.
Long Beach, California

Georgia Institute of Technology
School of Aerospace Engineering
Atlanta 13, Georgia
ATTN: Mr. D. W. Dutton

Vehicle Research Corporation
1661 Lombardy Road
Pasadena, California
ATTN: Dr. Scott Rethorst

University of Virginia
Aerospace Engineering Department
Charlottesville, Virginia
ATTN: Dr. G. B. Matthews

Mississippi State University
Engineering and Industrial Research
Station
State College, Mississippi
ATTN: Dr. J. J. Cornish

Vidya Division
1450 Page Mill Road
Stanford Industrial Park
Palo Alto, California
ATTN: Dr. J. N. Nielsen

Syracuse University
Mechanical Engineering Department
Syracuse, New York
ATTN: Dr. S. Eskinazi

Naval Postgraduate School
Aeronautical Engineering
Department
Monterey, California
ATTN: Dr. R. Head

Technical Library (Code P80962)
U. S. Naval Ordnance Test Station
Pasadena Annex
3202 E. Foothill Blvd.
Pasadena 8, California

Commanding Officer and Director
David Taylor Model Basin
Aerodynamics Laboratory
Washington, D. C. 20007
ATTN: Mr. H. Chaplin

Mr. Maurice Sevik
Ordnance Research Laboratory
Pennsylvania State University
P. O. Box 30
University Park, Pennsylvania

Mr. Paul Granville
Hydrodynamics Laboratory
David Taylor Model Basin
Code 581
Washington, D. C. 20007

Commanding Officer and Director
David Taylor Model Basin
Hydrodynamics Laboratory
Washington, D. C. 20007
ATTN: Dr. William B. Morgan